Correspondence

A Deconvolution Filter for Improvement of Time-Delay Estimation in Elastography

S. Kaisar Alam, *Senior Member, IEEE*, Jonathan Ophir, *Member, IEEE*, Ignacio Céspedes, *Member, IEEE*, and Tomy Varghese, *Member, IEEE*

***Abstract*—In elastography, tissue under investigation is compressed, and the resulting strain is estimated from the gradient of displacement estimates. Therefore, it is important to accurately estimate the displacements (time-delay) for good quality elastograms. A principal source of error in time-delay estimation in elastography is the decorrelation of the echo signal due to tissue compression (decorrelation noise). Temporal stretching of the postcompression signals has been shown to reduce the decorrelation noise at small strains. In this article, we present a deconvolution filter that reduces the decorrelation even further when applied in conjunction with signal stretching. The performance of the proposed filter is evaluated using simulated data.**

I. Introduction

ULTRASONIC imaging methods based on tissue elasticity have recently been investigated for diagnosis of disease [1]–[8]. Ultrasonic techniques to estimate strain due to externally applied compression have been developed [5], [6]. In these methods, the local tissue displacements are estimated from the time-delays of gated pre- and postcompression echo signals, which are then used to estimate the axial strain. In elastography [5], time-delays are estimated from the location of the peak of the cross-correlation function between the windowed pre- and postcompression echo signals.

The quality of elastograms is highly dependent on the quality of time-delay estimates. Time-delay estimation in elastography is corrupted primarily by two factors: random noise (electronic and quantization), and decorrelation due to tissue compression. We previously investigated the effect of temporal stretching [9]–[11] of the postcompression echo signals, and found it to significantly reduce axial decorrelation [9]. Correlation is improved because temporal stretching of the postcompression signal effectively realigns the scatterers. However, it also stretches the point-spread function (PSF) of the system that is involved in the generation of the echo signal, resulting in some residual decorrelations.

As we show in this paper, this can become a major problem. However, in the current applications of elastography, these errors may be masked by larger errors. Elastography involves tissue motion in three-dimensions. However, until recently, nonaxial motions have been ignored. Efforts are now underway to reduce decorrelation due to nonaxial tissue motion, and thus reduce the dimensionality of the problem. The errors due to PSF deformation become significant when the dimensionality of the problem is reduced. In this article, we demonstrate the correlation enhancement obtained by processing the postcompression signal with a deconvolution filter following the temporal stretching step.

We propose an inverse filter approach for the deconvolution. It can be shown that the inverse filter is a special case of the optimal Wiener filter that can be used in deconvolution problems. The Wiener filter can be expressed as follows [12]:

$$H_{\text{Wiener}}(f) = \frac{P^*(f)}{|P(f)|^2 + \frac{S_n(f)}{S_r(f)}}$$

where $P(f)$ is the transfer function of the system, $S_n(f)$ is the noise power spectral density, and $S_r(f)$ is the power spectral density of the random distribution that the scatterers are part of. Depending on the signal-to-noise ratio (SNR), there can be two extreme cases of this Wiener filter [13]. When the SNR is very high, $S_n(f)/S_r(f)$ can be neglected, and $P^*(f)$ cancels from the numerator and denominator, resulting in the classical inverse filter we have used in this paper:

$$H_{\text{inverse}}(f) = \frac{1}{P(f)}.$$

However, when noise dominates the signal, $|P(f)|^2$ can be neglected. Then the filter approaches a matched filter:

$$H_{\text{Match}}(f) = P^*(f)\frac{S_r(f)}{S_n(f)}.$$

In elastography, the associated SNR in the sonographic signals is generally high, and high sonographic SNR is necessary for relatively error-free displacement estimates for strain estimation. Thus, the inverse filter approach may be valuable in elastography.

II. Motivation

A. The Nonlinear Relation Between the Correlation Coefficient and the SNR

In elastography, strain is estimated from the gradient of displacement estimates. In pure time-delay estimation models, only noise corrupts the displacement estimates. In elastography, we need to compress the tissue in order to produce tissue strain; the compression itself introduces decorrelation in the postcompression signal. Thus, displacements need to be estimated in the presence of signal decorrelation, in addition to noise. This decorrelation is independent of the level of random noise, and earlier works have shown that decorrelation effects can be expressed as an SNR measure [14], [15]. A highly nonlinear relationship exists between decorrelation and the corresponding SNR. We have plotted the corresponding SNR vs. the correlation coefficient (ρ) in Fig. 1. We observe that, with the increase

Manuscript received February 9, 1998; accepted April 19, 1998. This work was supported in part by NIH Program Project grant P01-CA64597.

S. K. Alam is with the Riverside Research Institute, New York, NY 10036. J. Ophir and T. Varghese are with the Ultrasonics Laboratory, Radiology Department, The University of Texas Medical School, Houston, TX 77030 (e-mail: jophir@ msrad3.med.uth.tmc.edu).

I. Céspedes is with Endosonics Corporation, Rancho Cordova, CA 95670.

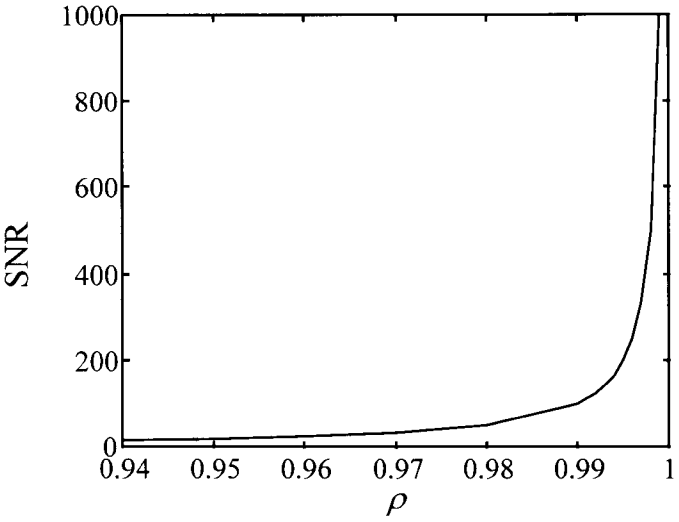

Fig. 1. Illustration of the effect of increasing the correlation coefficient on the corresponding SNR. Note the highly nonlinear behavior of the curve.

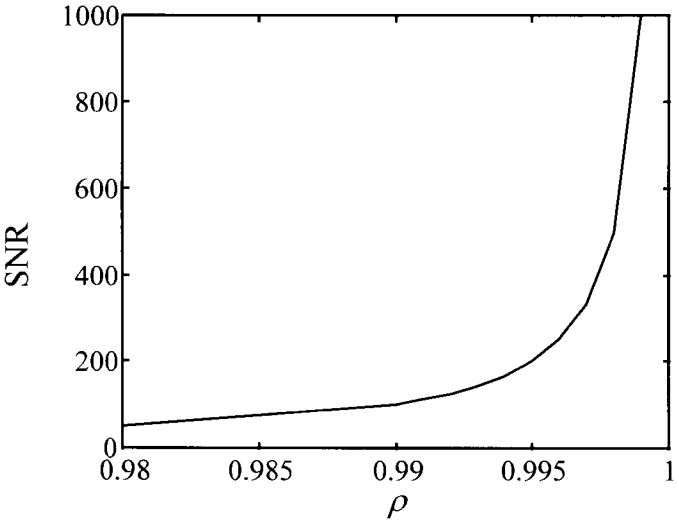

Fig. 2. Plotting the graph in Fig. 1 for $\rho \geq 0.98$. At ρ close to unity, the corresponding SNR increases very rapidly with the increase in ρ.

in ρ, the SNR increases much faster. In Fig. 2, we replot the figure for $\rho \geq 0.98$ only. We observe that at ρ close to unity, even a small improvement in ρ results in a significant increase in the SNR. As ρ increases by very small amounts from 0.96 to 0.98 to 0.99 to 0.995, the SNR more than doubles each time. It was reported earlier that, when correlation drops to below 0.93, phase ambiguities set in, sharply reducing the maximum achievable elastographic SNR (SNR_e) [16]. Thus, in partially decorrelated signals, reducing decorrelation is very important, especially when ρ is close to 0.93 and also close to unity.

B. Three-dimensional Motion in Elastography

The tissue undergoes a three-dimensional motion when subjected to external compression. However, until recently, all the work in elastography has implicitly assumed axial only tissue motion; and the effects due to nonaxial motion remained unaccounted for. Two recent papers [17], [18] have investigated the issue of nonstationarity associated with elastography. Kallel *et al.* [18] have shown that, after the postcompression echo signal is temporally stretched, the effective correlation between the pre- and postcompression echo signals can be expressed as follows:

$$\rho = \rho_E \times \rho_L \times \rho_A, \tag{1}$$

where ρ_E, ρ_L, ρ_A are the elevational, lateral, and axial correlation coefficients, respectively. In typically ignoring the nonaxial movements of the tissue, we make the implicit (albeit incorrect) assumption that $\rho_E = \rho_L = 1$. The axial decorrelation ($\rho_A \neq 1$) in the temporally stretched postcompression signal may have several sources: 1) frequency dependent attenuation in conjunction with changes in the beam and other effects, and 2) stretching of the PSF as shown in Alam and Ophir [9]. Thus the axial correlation ρ_A can be expressed as:

$$\rho_A = \rho_{A1} \times \rho_{A2}, \tag{2}$$

where ρ_{A1} and ρ_{A2} are the correlation coefficients from sources 1 and 2, respectively. Note that ρ_E, ρ_L and ρ_{A1} refer to three sources of nonstationarity in elastography. The correction for the 3-D motion is very difficult because of the unpredictable nature of the nonstationarities. Konofagou and Ophir [19] have recently shown that, even under carefully designed boundary conditions, the nonaxial displacements are poorly controlled and may not be well behaved. This is due to the fact that, even small changes in boundary conditions can have substantial effects on the nonaxial displacements, which in turn can have even bigger effects in the achievable correlations. Small details such as how the sample is held, how lubricated the compressor and the floor are, or whether the compressor is perfectly parallel to the floor may have unexpected consequences. Recent works [19]–[21] have shown that it is possible to dramatically reduce these errors, but further work is necessary to fully develop these methods.

After all the decorrelations due to various nonstationarities have been removed ($\rho_E = \rho_L = \rho_{A1} = 1$), the decorrelation due to the stretching of the PSF will still be present ($\rho_{A2} \neq 1$), especially at larger strains (however, stretching is essential because the improvement from stretching is greater than the degradation from the change in the PSF, and without stretching, the displacement estimates contain very large errors at large applied strain). Thus, the decorrelation from PSF deformation will be a major source of performance degradation (as will also be shown in this paper) after other sources of the nonstationarity in the three dimensions are removed or considerably reduced. A suitably designed deconvolution filter can further reduce this decorrelation.

III. Theory

A. Deconvolution Filtering of the Temporally Stretched Postcompression Signal

In a homogeneous target, the zero-mean pre- and postcompression echo signals can be modeled in one-dimension by:

$$r_1(t) = s_1(t) + n_1(t) = s(t) * p(t) + n_1(t), \tag{3a}$$

$$r_2(t) = s_2(t) + n_2(t) = s\left(\frac{t}{a} - t_0\right) * p(t) + n_2(t), \tag{3b}$$

and the temporally stretched postcompression signal can be expressed as:

$$r_3(t) = r_2(at) = s_3(t) + n_3(t) = as(t - t_0) * p(at) + n_3(t). \tag{3c}$$

where $s(t)$ is the zero-mean one-dimensional scattering distribution of the elastic target, $p(t)$ is the impulse response of the ultrasonic system, $n_1(t)$ and $n_2(t)$ are uncorrelated random noise and $*$ denotes convolution. The quantity $n_3(t)$ is a time-scaled version of $n_2(t)$. The quantity a is related to the tissue strain ε by the simple relationship:

$$a = 1 - \varepsilon. \tag{4}$$

From (3a) and (3c), we observe that in $r_3(t)$ the effect of scatterer compression has been compensated, but the system impulse response also has been temporally stretched. Nevertheless, temporal stretching generally improves the correlation between the pre- and postcompression signals [9]. It is because the scatterer profile varies faster than the impulse response, and thus compression of the former introduces more decorrelation than stretching of the latter.

Evaluating the Fourier transform of $r_1(t)$ and $r_3(t)$:

$$R_1(f) = S_1(f) + N_1(f) = S(f)P(f) + N_1(f), \tag{5a}$$

and

$$R_3(f) = S_3(f) + N_3(f) = S(f)P\left(\frac{f}{a}\right)e^{-j2\pi f t_0} + N_3(f). \tag{5b}$$

Under noiseless conditions,

$$R_3(f) = S(f)P\left(\frac{f}{a}\right)e^{-j2\pi f t_0}. \tag{6}$$

If we define a filter $H(f) = \frac{P(f)}{P(f/a)}$ for deconvolving $R_3(f)$, then,

$$\begin{aligned} R_{3-\text{deconv.}}(f) &= R_3(f)H(f) = S(f)P\left(\frac{f}{a}\right)e^{-j2\pi f t_0}\frac{P(f)}{P(f/a)} \\ &= S(f)P(f)e^{-j2\pi f t_0} = S_1(f)e^{-j2\pi f t_0}. \end{aligned} \tag{7}$$

Thus,

$$r_{3-\text{deconv.}}(t) = s_1(t - t_0) = r_1(t - t_0). \tag{8}$$

Thus, under ideal circumstances (no noise or attenuation), it is possible to reconstruct the stretched signal perfectly as long as the system transfer function $P(f)$ is known and it does not have any zeroes in the frequency range of interest. Note that for a Gaussian impulse response, the filter is a high frequency emphasis filter as will be evident in (13). Now, with noise present, if the deconvolution filter is applied,

$$\begin{aligned} R_{3-\text{deconv.}}(f) &= R_3(f)H(f) = \{S_3(f) + N_3(f)\}\frac{P(f)}{P(f/a)} \\ &= S_1(f)e^{-j2\pi f t_0} + N_3(f)\frac{P(f)}{P(f/a)}. \end{aligned} \tag{9}$$

The above equation can be written a little differently:

$$\begin{aligned} R_{3-\text{deconv.}}(f) &= \{S_3(f) + N_3(f)\}H(f) \\ &= S_3(f)\left\{1 + \frac{N_3(f)}{S_3(f)}\right\}H(f) \\ &= S_3(f)\left\{1 + \frac{1}{\text{SNR}(f)}\right\}H(f). \end{aligned} \tag{10}$$

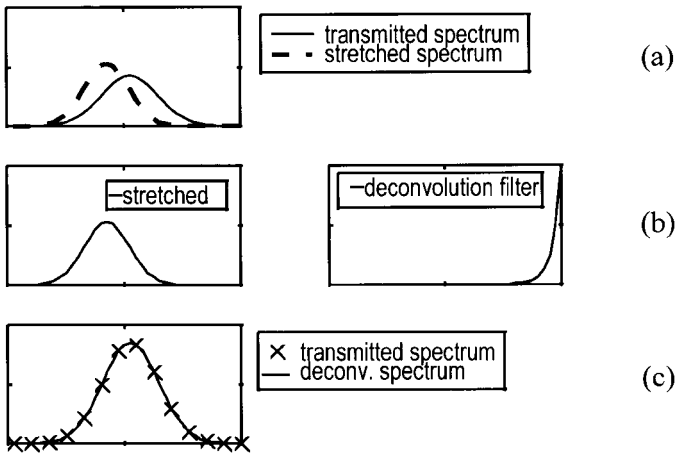

Fig. 3. Illustration of deconvolution filtering.

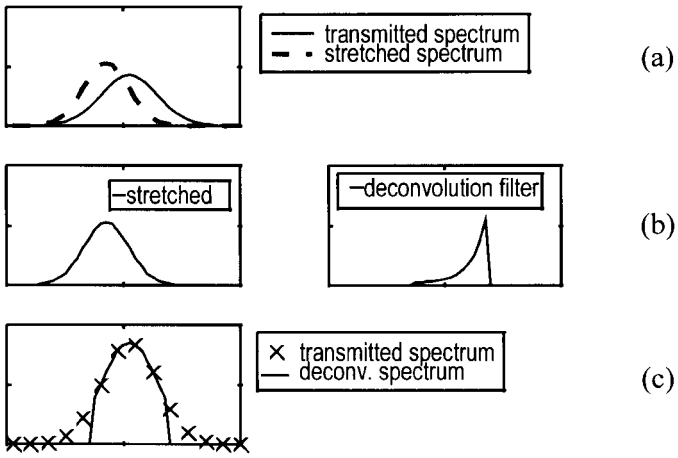

Fig. 4. Illustration of deconvolution filtering, a threshold is applied because of noise, and the resulting spectrum has a smaller support.

By examining (10), we observe that care should be taken when applying this deconvolution filter to noisy signals. The deconvolution filter should be applied only in the frequency range where the SNR is greater than unity. Amplification in the region in which noise dominates the signal is not desirable. Thus, the deconvolution filter should be designed as follows:

$$H(f) = \begin{cases} \frac{P(f)}{P(f/a)}, & |S_3(f)| \geq |N_3(f)| \text{ and } P(f/a) \neq 0 \\ 0, & \text{otherwise.} \end{cases} \tag{11}$$

The concept of deconvolution filtering is illustrated in Figs. 3 and 4. In Fig. 3, we show the ideal case. Fig. 1(a) shows $P(f)$ and $P(f/a)$. Fig. 3(b) shows $P(f/a)$ and $H(f)$. Fig. 3(c) shows the original and equalized spectra, and they are virtually identical. Fig. 4 has the same pictures, but, this is for a case in which the noise in the signal raised the threshold. The resulting equalized transfer function has a smaller support than the original. However, the original and the equalized spectra are virtually identical in the nonzero region.

It can be shown that, for a system with a Gaussian PSF,

$$p(t) = 2\sqrt{2\pi}\sigma e^{-2(\pi\sigma t)^2}\sin(2\pi f_0 t), \tag{12}$$

the deconvolution filter can be expressed as:

$$H(f) = \frac{P(f)}{P(f/a)} = e^{\frac{(1-a^2)f^2}{2(a\sigma)^2}} \frac{\sinh(ff_0/\sigma^2)}{\sinh(ff_0/a\sigma^2)}. \qquad (13)$$

B. Deconvolution Filtering of the Cross-correlation Functions

We may improve the performance of the time-delay estimator using a deconvolution filter if the local strain and the system impulse response are known. Because both filtering and correlation are linear operations, the order can be reversed. If the cross-correlation function is passed through the filter $H(f)$, then

$$\begin{aligned} G_{13-\text{deconv.}}(f) &= G_{13}(f)H(f) \\ &= G_{11}(f)\frac{P(f/a)}{P(f)}e^{-j2\pi ft_0}\frac{P(f)}{P(f/a)} \\ &= G_{11}(f)e^{-j2\pi ft_0}, \end{aligned} \qquad (14)$$

where $G_{13}(f)$ is the cross-spectrum between the precompression echo signal and the temporally stretched postcompression signal and $G_{11}(f)$ is the autospectrum of the precompression signal. It must be noted that reversing the order of filtering and correlation operations can be done for unnormalized correlation functions only. Normalized correlation functions are not linear, and so the order of operations cannot be reversed.

C. Sensitivity Analysis with Respect to the Center Frequency and Bandwidth

When a tissue is investigated using an ultrasonic pulse, both the center frequency and bandwidth change with the propagation of the pulse. The center frequency decreases with depth due to frequency dependent scattering and attenuation. The ultrasonic pulse elongates away from the focus due to varying arrival time from various sections of the transducer, resulting in reduced bandwidth. If deconvolution filtering has a strong dependence on accurately specifying the center frequency and bandwidth, then its practical utility is dubious. The dependence of $H(f)$ on f_0 and σ can be shown to be:

$$\frac{\partial H}{\partial f_0} \approx \frac{f}{\sigma^2}\left(1-\frac{1}{a}\right)e^{\frac{(1-a^2)f^2}{2(a\sigma)^2}}e^{(1-1/a)ff_0/\sigma^2},$$

and

$$\frac{\partial H}{\partial \sigma} \approx -2\left\{\frac{ff_0}{\sigma^3}\left(1-\frac{1}{a}\right)+\frac{(1-a^2)f^2}{2a^2\sigma^3}\right\} \times e^{\frac{(1-a^2)f^2}{2(a\sigma)^2}}e^{(1-1/a)ff_0/\sigma^2}.$$

At $f_0 = 5$ MHz, 60% bandwidth and 1% strain $\left.\frac{\partial H/\partial f_0}{H(f)}\right|_{f=f_0} = -0.035$/MHz and $\left.\frac{\partial H/\partial \sigma}{H(f)}\right|_{f=f_0} = -0.0015$/MHz. These values change to -0.0709/MHz and -0.0060/MHz, respectively, at 2% strain. At 5% strain, these values are -0.1827/MHz and -0.0401/MHz, respectively. Thus, the deconvolution filter is more sensitive to changes in the center frequency than the bandwidth. But, the sensitivity is small enough to not drastically affect the performance. We plot $H(f)$ at 2% strain for some variations in values of center frequency and bandwidth used in the deconvolution filter when the true values were the 5 MHz and 60% in Figs. 5 and 6. Clearly, we do not observe significant variations in the filter as a result. We normally do not expect any drastic changes in the center frequency and bandwidth due to frequency-dependent attenuation and focusing effects.

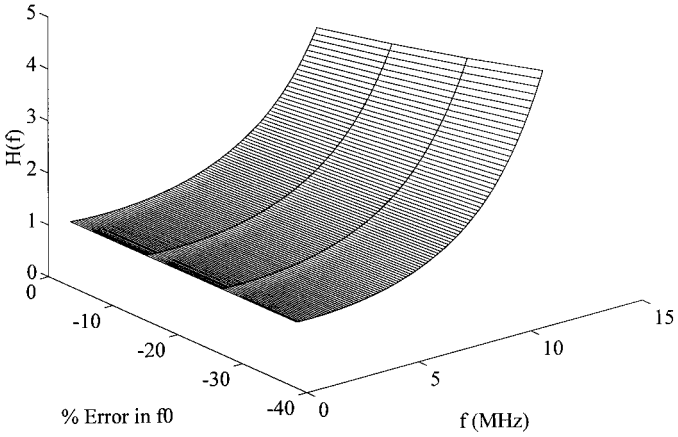

Fig. 5. Illustration of changes in the deconvolution filter when the center frequencies are not accurate. $f_0 = 5$ MHz, BW = 60%.

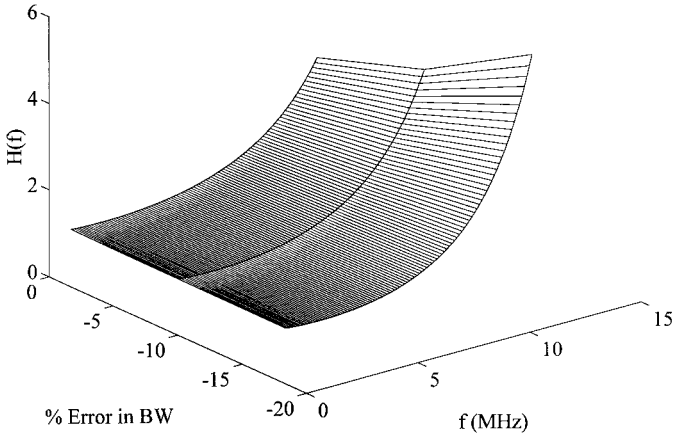

Fig. 6. Illustration of changes in the deconvolution filter when the bandwidths are not accurate. $f_0 = 5$ MHz, BW = 60%.

IV. Simulation

We performed 1-D simulations using MATLAB[1] to verify the theory. We simulated a line of uniformly spaced random amplitude (Gaussian distributed) scatterers within a transducer beam (10 scatterers per wavelength). For the simulated round-trip PSF, the center frequency was 5 MHz, and the noise equivalent bandwidth was 60%. The RF A-line was computed by convolving the scatterer profile with the PSF. The A-lines were sampled at 500 MHz. The scatterer spacing was then appropriately reduced to simulate tissue compression, and the RF A-line was recomputed. Then, this RF A-line was temporally stretched by the factor by which the scatterer spacing had been reduced. We have added white noise to the RF A-lines to get a predetermined sonographic SNR. And, an appropriate deconvolution filter was applied on the temporally stretched postcompression A-line. To test how well deconvolution filtering performed, we computed the autocorrelation function for the

[1]MATLAB is a registered trademark of The MathWorks, Inc., Natick, MA.

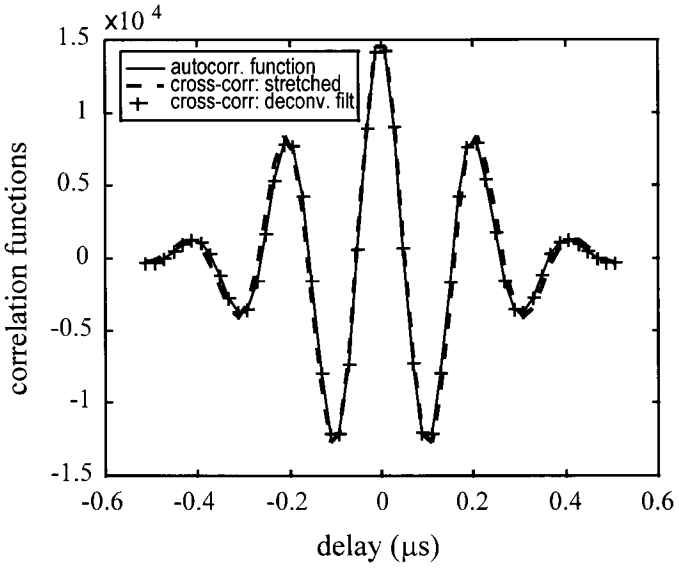

Fig. 7. Correlation functions: 5% strain, SNR = 60 dB.

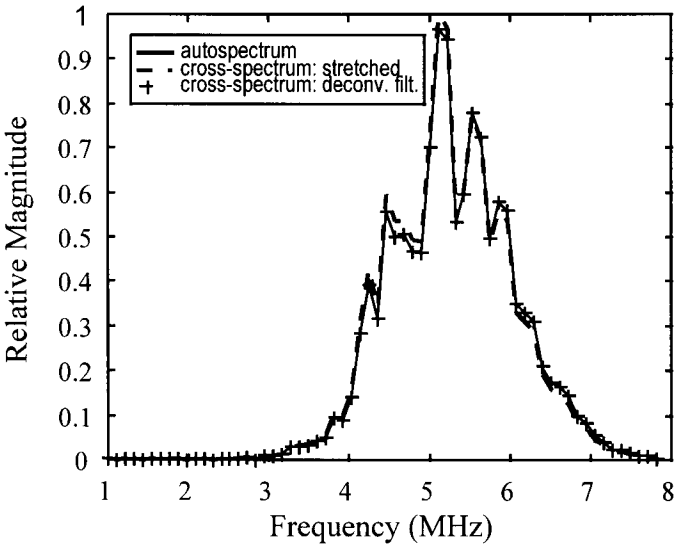

Fig. 8. Auto and cross-spectra: 2% strain, SNR = 60 dB.

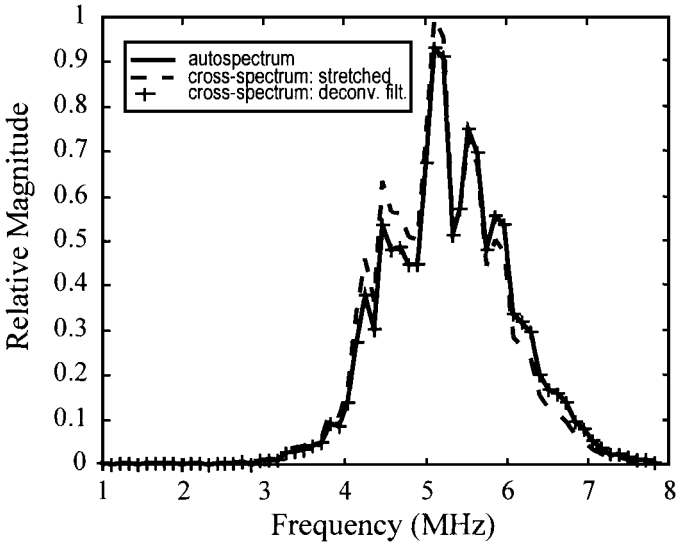

Fig. 9. Auto and cross-spectra: 5% strain, SNR = 60 dB.

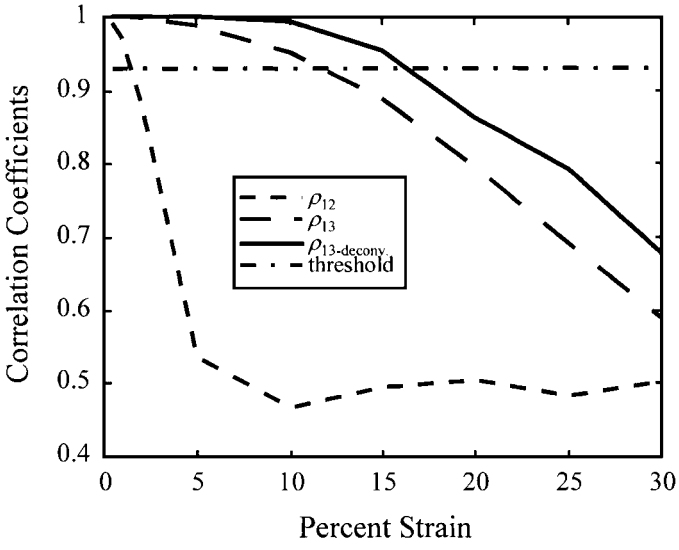

Fig. 10. Improvement in correlation due to deconvolution: 5% strain, SNR = 60 dB.

precompression A-line $C_{11}(f)$ and the cross-correlation function between the pre- and the postcompression A-lines $C_{12}(f)$, between the precompression A-line and the stretched postcompression A-line $C_{13}(f)$, and also between the precompression A-line and the deconvolution filtered postcompression A-line $C_{13-\text{deconv.}}(f)$. A window size of 5.12 μs was used for the correlation operations. These correlation functions were averaged over 16 realizations. Fourier transformations of the correlation functions were taken to get the auto- and cross-spectra. We also computed the correlation coefficient for all the cases, with window size of 2 μs, averaged over 32 realizations.

V. Results

The results for the 1-D simulation described in the previous section are shown in Figs. 7–14. the SNR was 20 dB. The unnormalized cross-correlation function can mask the difference between the signals due to averaging of the uncorrelated noise implicit in the correlation operations, and thus, may hide some dissimilarities between them. Computing the correlation coefficients between different signals reveals the true similarities between the signals and has been performed. However, for the sake of completeness, we begin by plotting the unnormalized correlation functions and cross-spectra. In Fig. 7, correlation functions are plotted for an applied strain of 5%. At this strain level, stretching cannot fully compensate for the tissue strain, and a visible difference exists between the cross-correlation function between the precompression and temporally stretched postcompression signals C_{13} and the autocorrelation function for the precompression signal C_{11}. However, the cross-correlation function between the precompression and deconvolution filtered temporally stretched postcompression signals $C_{13-\text{deconv.}}$ is almost indistinguishable from C_{11}. We reemphasize that the apparent small improvement in the correlation due to stretching can be misleading, because even a small increase in the correlation may significantly improve the estimator performance, especially at lower strains [14]. The sonographic SNR was 60 dB for the cases shown in Figs. 7–10. In Fig. 11,

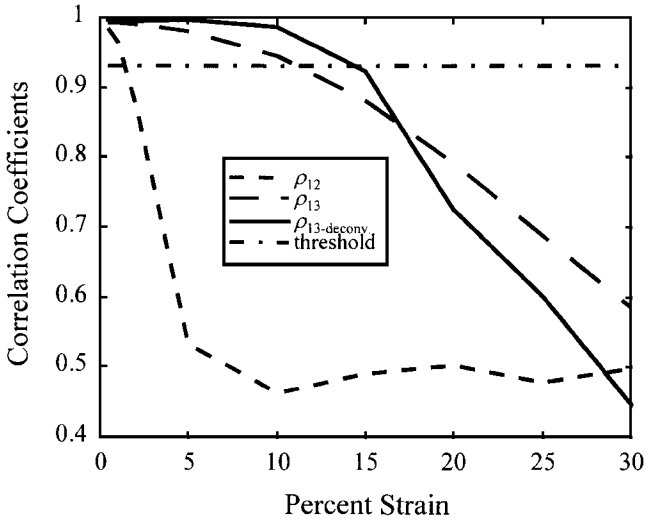

Fig. 11. Improvement in correlation due to deconvolution: 5% strain, SNR = 20 dB.

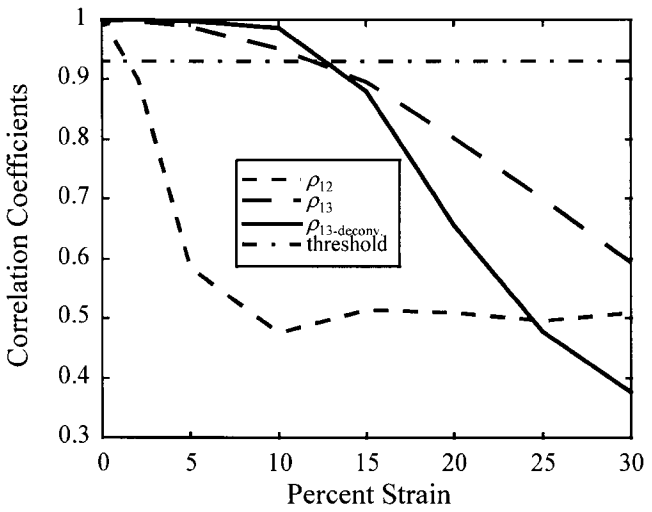

Fig. 12. Improvement in correlation due to deconvolution. Center frequency used in the filter = 5 MHz, true center frequency = 4.5 MHz.

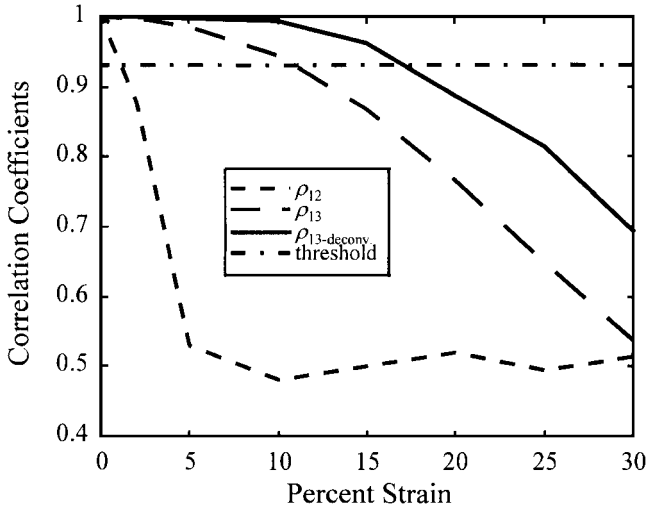

Fig. 13. Improvement in correlation due to deconvolution. Bandwidth used in the filter = 60%, true bandwidth = 55%.

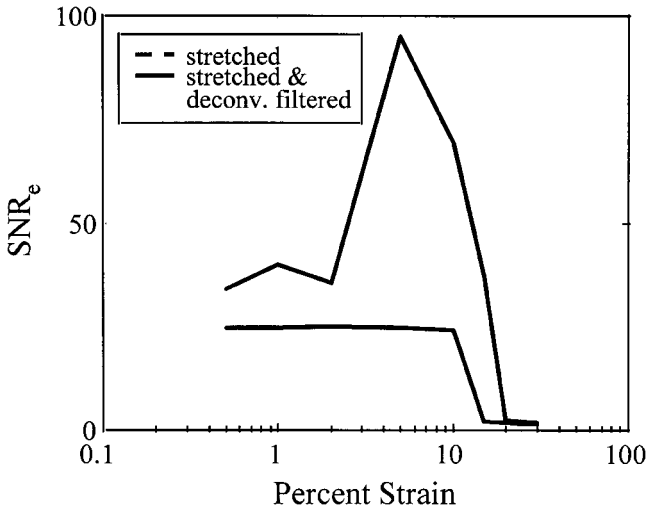

Fig. 14. Improvement in the strain filters due to deconvolution. The area under the strain filter may be regarded as a generalized quality measure of an elastogram. The same correlation values from Fig. 10 were used to generate the strain filters. Note that a moderate increase in the correlation translates into a large increase in the achievable elastographic SNR_e. Note also that the onset of the Barankin bound is shifted toward higher strains.

Figs. 8 and 9 show the corresponding spectral behavior at 2% and 5% strains. In Fig. 8, at 2% strain, the cross-spectrum for the unstretched case G_{13} is a slightly lowpass filtered version of the autospectrum G_{11}, due to the stretching of the impulse response itself. The cross-spectrum for the deconvolution filtered case $G_{13-\text{deconv.}}$ and the autospectrum G_{11} becomes virtually indistinguishable. The deconvolution filter continues to perform well at 5% strain, shown in Fig. 9. At higher strains, the performance has shown degradation; however, those cases are not shown for the sake of brevity and lack of utility of very large strains.

If uncorrelated noise is added to two identical signals, the unnormalized correlation function averages out the uncorrelated noise in the signals, and may not fully show the true dissimilarities between them. Indeed, differences between the cases with and without deconvolution filtering are present but are not striking in Figs. 7–9. To expose their true dissimilarity, we may have to evaluate the normalized correlation coefficient. So, we also have computed the correlation coefficients between different signals to evaluate the true similarities between the signals and plotted them vs. strain. At a sonographic SNR of 60 dB (Fig. 10), the improvement in the correlation from stretching and deconvolution filtering is apparent. The correlation coefficient falls below the important threshold of 0.93 [16] at strains lower than 2% when stretching is not applied, higher than 10% when stretching is applied, and higher than 15% when deconvolution filtering is applied. Thus, deconvolution filtering gives us a sizable boost in maximum usable strains. At all strain levels $\rho_{13-\text{deconv.}} > \rho_{13} > \rho_{12}$. As demonstrated in Figs. 1 and 2, even small increases in correlation coefficients can have a significant effect on the SNR_e. We will demonstrate the effect that deconvolution filtering will have on the upper bounds of SNR_e in another graph. At a sonographic SNR of 20 dB (Fig. 11), all the correlation values are slightly smaller. But, the deconvolution filter still improves the correlation for strains up to $\sim 15\%$. Above that strain, the deconvolution filter in fact degrades the

performance. However, in elastography, our interest is mainly limited to lower strains, and the sonographic SNR values are generally high.

To apply the deconvolution filter properly, we need to know the $P(f)$, and especially its center frequency. Because the PSF is generally nonstationary due to the effects of decorrelation and frequency dependent attenuation, a perfect correction for the changes in $P(f)$ may not be possible. However, as discussed in the theory section, even if there are some errors in the assumption of center frequency and bandwidth, deconvolution filtering produces perceivable improvements as long as the values used are not very different from the true values. These effects are shown in Figs. 12 and 13, which are otherwise similar to Figs. 10 and 11. In Fig. 12 the deconvolution filter uses a center frequency of 5 MHz, whereas the true center frequency is 4.5 MHz (10% drop). For this case, the deconvolution filter is still able to improve signal correlation up to about a strain of 12%. Beyond this, stretching alone performs better. In Fig. 13 the deconvolution filter uses a bandwidth of 60%, whereas the true bandwidth is 55% (8% drop). However, the incorrect bandwidth does not have a very adverse effect on the deconvolution filter. The results support the conclusions in Section III that bandwidth has a less pronounced effect on deconvolution filtering.

To demonstrate the true effect of deconvolution filtering, we used the correlation values for Fig. 11 and converted them into a maximum achievable SNR_e measure using the strain filter formulation [16]. The strain filter consists of an analytical and graphical representation of the "quality" of strain estimates vs. strain for a set of system and processing parameters. The width of the strain filter provides the dynamic range and its height the respective SNR_e value of the estimated strain. The strain filter has three identifiable regions: 1) the Cramér-Rao lower bound (CRLB) region, where the displacement estimation errors are mainly jitter errors around the true peak; 2) the Barankin bound (BB) region, where phase ambiguity (or peak errors) introduces large errors in the displacement estimation, resulting in sharply lower SNR_e (this also generally denotes the high strain end of the elastographic dynamic range); and 3) the constant variance (CV) region, where both amplitude and phase ambiguities occur and the estimates are largely useless. The strain filters with and without deconvolution filtering are shown in Fig. 14. Deconvolution filtering produces two clear effects. The seemingly modest increase in the correlation coefficient derived from deconvolution filtering results in a significant increase in the height of strain filters. The improvement in the SNR_e is at all strain values, but it is especially pronounced for strains larger than 2%. This could be significant, because sometimes it is necessary to apply larger strains to increase the elastographic dynamic range [22]. It also may be important when elastographically visualizing soft areas that incur large strains. A second effect is that the maximum strains that can be measured with a reasonable SNR_e also increases as the Barankin region is shifted toward higher strains. If we compare Figs. 10 and 14, we observe that, although Fig. 14 shows the improvement from deconvolution filtering much more clearly, the same effects also are present in Fig. 10. Overall, the improvement in the strain filter, and hence in the underlying elastograms, due to deconvolution filtering is quite significant, even due to the corresponding small improvements in the signal correlation.

VI. Conclusion

Echo-signal decorrelation is one of the major limiting factors in strain estimation and imaging. Elastography involves tissue motion in all three dimensions. Recent works [18]–[21] suggest that it is possible to significantly improve the elastograms by paying attention to the three-dimensional nature of tissue motion. Various methods have been proposed to reduce decorrelations from the nonaxial tissue motion [19]–[21]. When these effects are corrected for, the residual decorrelation resulting from the deformation of the PSF in the temporal stretching operation becomes significant. We have presented a deconvolution filter that can compensate for the undesired stretching of the PSF. The 1-D simulation results show the effectiveness of deconvolution filtering. The deconvolution filter improves the correlation between the precompression and stretched signals. We have also demonstrated using strain filters (that describes the upper bounds in SNR_e) computed from the same correlation values that these seemingly modest improvement in correlation from deconvolution filtering results in significant improvement in SNR_e.

We have investigated the effect of small errors in estimating the center frequency and bandwidth on deconvolution filtering. Both were found to increase the errors only by a small amount, but error in bandwidth was found to introduce less error. We speculate that this is due to the fact that the energy at the tail ends of the spectrum is low to begin with. Small changes in the bandwidth mostly affect the tail ends, and do not change the deconvolution filter significantly.

In inhomogeneous tissues, local strains vary, and thus a global uniform temporal stretching is not ideal. We have proposed a novel estimator in which the proper local stretch factor is estimated using an iterative procedure [23], and deconvolution filtering may be useful here. However, we also have observed that a uniform temporal stretching generally produces low-noise elastograms unless both the following conditions are true: the applied strain is large, and strain contrast is large. In fact, it is an "efficient" strain estimator because it is not computationally intensive and produces low-noise elastograms in most cases. Inverse filtering may be useful in the future in conjunction with temporal stretching to further reduce the noise in the elastograms after the methods to correct for the 3-D motion [19]–[21] are fully developed.

References

[1] T. A. Krouskop, D. R. Dougherty, and F. S. Vinson, "A pulsed Doppler ultrasonic system for making noninvasive measurements of the mechanical properties of soft tissue," *J. Rehab. Res. Dev.*, vol. 24, pp. 1–8, 1987.

[2] R. M. Lerner, S. R. Huang, and K. J. Parker, "'Sonoelasticity' images derived from ultrasound signals in mechanically vibrated tissues," *Ultrason. Med. Biol.*, vol. 16, pp. 231–239, 1990.

[3] R. M. Lerner and K. J. Parker, "Sono-elasticity in ultrasonic tissue characterization and echographic imaging," in *Proc. 7th Eur. Comm. Workshop*, J. M. Thijssen, Ed., Nijmegen, The Netherlands, 1987.

[4] Y. Yamakoshi, J. Sato, and T. Sato, "Ultrasonic imaging of internal vibration of soft tissue under forced vibration," *IEEE Trans. Ultrason., Ferroelect., Freq. Contr.*, vol. UFFC-47, pp. 45–53, 1990.

[5] J. Ophir, I. Céspedes, H. Ponnekanti, Y. Yazdi, and X. Li, "Elastography: A method for imaging the elasticity in biological tissues," *Ultrason. Imaging*, vol. 13, pp. 111–134, 1991.

[6] M. O'Donnell, A. R. Skovoroda, B. M. Shapo, and S. Y. Emelianov, "Internal displacement and strain imaging using ul-

trasonic speckle tracking," *IEEE Trans. Ultrason., Ferroelect., Freq. Contr.*, vol. UFFC-41, pp. 314–325, 1994.

[7] S. K. Alam, D. W. Richards, and K. J. Parker, "Detection of intraocular pressure change in the eye using sonoelastic Doppler ultrasound," *Ultrason. Med. Biol.*, vol. 20, pp. 751–758, 1994.

[8] D. J. Rubens, M. A. Hadley, S. K. Alam, L. Gao, R. D. Mayer, and K. J. Parker, "Sonoelasticity imaging of prostate cancer: *In vitro* results," *Radiology*, vol. 195, pp. 379–383, 1995.

[9] S. K. Alam and J. Ophir, "Reduction of signal decorrelation from mechanical compression of tissues by temporal stretching: applications to elastography," *Ultrason. Med. Biol.*, vol. 23, pp. 95–105, 1997.

[10] I. Céspedes, "Elastography: imaging of biological tissue elasticity," Ph.D. dissertation, Univ. Houston, TX, 1993.

[11] I. Céspedes and J. Ophir, "Reduction of image noise in elastography," *Ultrason. Imaging*, vol. 15, pp. 89–102, 1993.

[12] M. Fatemi and A. C. Kak, "Ultrasonic B-scan imaging: Theory of image formation and a technique for restoration," *Ultrason. Imaging*, vol. 2, pp. 1–47, 1980.

[13] B. Haider, P. A. Lewin, and K. E. Thomenius, "Pulse elongation and deconvolution filtering for medical ultrasonic imaging," *IEEE Trans. Ultrason., Ferroelect., Freq. Contr.*, vol. 45, pp. 98–113, 1998.

[14] I. Céspedes, J. Ophir, and S. K. Alam, "The combined effect of signal decorrelation and random noise on the variance of time delay estimation," *IEEE Trans. Ultrason., Ferroelect., Freq. Contr.*, vol. 44, pp. 220–225, 1997.

[15] B. H. Friemel, "Real-time ultrasonic two-dimensional vector velocity estimation utilizing speckle-tracking algorithms: implementation and limitations," Ph.D. dissertation, Duke Univ., Durham, NC, 1994.

[16] T. Varghese and J. Ophir, "A theoretical framework for performance characterization of elastography: The strain filter," *IEEE Trans. Ultrason., Ferroelect., Freq. Contr.*, vol. 44, pp. 164–172, 1997.

[17] ——, "The nonstationary strain filter in elastography. Part I. Frequency dependent attenuation," *Ultrason. Med. Biol.*, vol. 23, pp. 1343–1356, 1997.

[18] F. Kallel, T. Varghese, J. Ophir, and M. Bilgen, "The nonstationary strain filter in elastography. Part II. Lateral and elevational decorrelation," *Ultrason. Med. Biol.*, vol. 23, pp. 1357–1369, 1997.

[19] E. E. Konofagou and J. Ophir, "A new elastographic method for estimation and imaging of lateral displacements, lateral strains, corrected axial strains, and Poisson's ratios in tissues," *Ultrasound Med. Biol.*, vol. 24, pp. 1183–1199, 1998.

[20] P. Chaturvedi, M. F. Insana, and T. J. Hall, "2-D companding for noise reduction in strain imaging," *IEEE Trans. Ultrason., Ferroelect., Freq. Contr.*, vol. 45, pp. 179–191, 1998.

[21] P. Chaturvedi, M. F. Insana, T. J. Hall, and M. Bilgen, "3-D companding using linear arrays for improved strain imaging," *1997 IEEE Ultrasonics Symposium Proceedings*, pp. 1435–1438, 1997.

[22] E. E. Konofagou, J. Ophir, F. Kallel, and T. Varghese, "Elastographic dynamic range expansion using variable applied strains," *Ultrason. Imaging*, vol. 19, pp. 145–166, 1997.

[23] S. K. Alam, J. Ophir, and E. E. Konofagou, "An adaptive strain estimator for elastography," *IEEE Trans. Ultrason., Ferroelect., Freq. Contr.*, vol. 45, pp. 461–472, 1998.